Kufa Journal of Engineering
Vol. 16, No. 4, October 2025, P.P. 288-301
Article history: Received 23 September 2024, last revised 28 January 2025, accepted 28 January 2025

PRESSURE LOSS COEFFICIENT OF LAMINAR FLOW ACROSS 30°, 45° AND 60° MINI MITRE BENDS

Wameedh T.M. Al-Tameemi [1], Mohammed Ridha Jawad Al-Tameemi [2], and Ahmed Jameel Khudhair [3]

[1] Department of Architectural Engineering, University of Diyala, 32001 Diyala, Iraq
Email: wameedh.altameemi@uodiyala.edu.iq

[2] Department of Mechanical Engineering, University of Diyala, 32001 Diyala, Iraq
Email: mohammedridha_eng@uodiyala.edu.iq

[3] Middle Technical University (MTU), Technical Institute of Baquba, Diyala, Iraq
Email: alkhalisa@mtu.edu.iq

https://doi.org/10.30572/2018/KJE/160417

ABSTRACT

Pressure loss coefficient of laminar flow across 30°, 45° and 60° mini scale mitre bends investigated for the first time by using CFD simulation. Various flow velocities between 0.05 and 2.2 m/s and three different pipes' diameters 1, 2 and 3mm were used to obtain laminar flow with Reynolds numbers range between 150 and 2190 for each mitre angle. More than one hundred case studies were used in the study. The extracted data from the simulation were employed to compute the key values theoretically for each case. The friction factor results of the present work agrees with the experimental values from the literature with less than ±5 % average error. The obtained data of mitre bends's pressure drop illustrate the independency of the Pressure coefficient K on both of the flow Reynolds numbers and the pipe diameter for the employed pipe sizes and flow conditions. The results obtained from this work verify the independent influence of the mitre angle on the pressure loss coefficient. New values of pressure loss coefficient for mini mitre bends are found, and they have 39-59% larger values than those for normal size mitre conduits.

KEYWORDS

Laminar flow, Mini pipes, Minor losses, Mitre bends, Pressure loss coefficient.

1. INTRODUCTION

Prediction of pressure loss throughout pipe conduits is crucial to the industrial piping networks designers for using these systems effectively (Spedding et al., 2004). Mitre bends with different mitred angles and pipe sizes are used in many systems for directing the flow towards the route of the piping network for the cases of space limitation (Munson et al., 2006). Mini size pipes (with diameters of 200μm < D*< 3mm (Mortazavi and Tajiri, 2015) are used in many applications such as heat sink and air conditioning systems, refrigeration, cooling systems and many other applications (Kim and Mudawar, 2013, Parmar et al., 2017, Wen et al., 2018, Li and Hibiki, 2017, Zhang et al., 2023, Sukamta et al., 2023, Al-Sayyab, 2018, Salih and Yaseen, 2020). (Symbols with * are dimensional quantities and the symbols without * are dimensionless).

Pressure drop across mitre bends is more complex compared with round bends due to the flow separation and back flow in the mitre bend as a result of secondary flow in addition to the frictional pressure drop. Pressure loss in bends is expressed in terms of pressure loss coefficient K. Due to the difficulties of conducting experimental investigations to examine the flow pressure loss in mini-scale pipes, researchers employ CFD as an effective alternative to study fluid flow and heat transfer through mini piping systems (Liu et al., 2012, Versteeg and Malalasekera, 1995, Debnath et al., 2017).

Pressure drop across mitre bends in normal pipes scale was examined experimentally and numerically in various studies in the literature (Al-Tameemi and Ricco, 2018, Haidar, 1995, Kirchbach, 1935, Schmandt and Herwig, 2013, Schmandt and Herwig, 2016, Schubart, 1935). Haidar (1995) studied the pressure loss coefficient of high turbulent flow across 30°, 60°, 90°, 120° and 150° single mitre bends. Pipe diameter of 40mm was employed in the investigation with Reynolds number Re=2×105. The study established that the coefficient of pressure drop has approximately constant value for each mitre angle at high turbulent flow.

Pressure loss coefficient of turbulent flow (Re> 27000) across single and multi-mitred bends investigated by Kirchbach (1935) for smooth pipes and by Schubart (1935) for rough pipes. These studies employed mitre bends with 43mm pipe diameters and various single and multi mitre angles. The studies reported that the pressure loss coefficient K across mitred bends does not depend on the Reynolds number for the applied boundary conditions. Crane (1988) reported that the pressure drop coefficient of mitre bends is directly relying on the friction factor Cf for each mitre angle.

Similarly, many fluid mechanics references (Munson et al., 2006, Rennels, 2022, White et al., 2011, Miller, 1990) reported a constant value of the coefficient K for each mitre angle regardless of the flow Reynolds number Re.

Donaldson et al. (2011) investigated the pressure drop in straight pipes and across round serpentine mini-channel with 1mm diameter. The study employed various flow velocities with Reynold number Re between 350 and 3900. The results showed that the pressure drop across the mini bends are affected by the flow Reynolds number and the curvature of the bends.

Ghobadi and Muzychka (2014) conducted an experimental study to examine the pressure drop of laminar flow through mini scale coiled tubes. The study utilised three different diameters 1.59mm, 1.27mm and 1.016mm for various flow conditions. The study found that the pressure drop through the coiled pipe was directly proportional with the increase of the flow Reynolds number. However, the pressure drop decreased with the increase of the curvature radius of the coiled tube for the same tube diameter.

Yusof et al. (2020) examined the pressure drop across serpentine mini scale rectangular channel numerically. The study utilised ANSYS Fluent to simulate the pressure drop of laminar flow across the bends. Various flow velocities were examined in the study with Reynolds numbers Re<2300. The results of the investigation depicted that the pressure loss coefficient of the serpentine decreased with the increase of Reynolds number Re.

It can be noticed that the studies of pressure drop across mini scale bends are limited to the serpentines and the round bends. To the best of the authors knowledge, there is no investigation in the open literature, have studied the pressure loss of laminar flow throughout mini-scale mitre bends. Therefore, the authors are motivated to conduct this work due to the importance of the pressure drop prediction across mini-scale mitre bends. The main purpose of the study is to investigate the drop of laminar flow pressure throughout 30°, 45° and 60° mini scale mitre bends in terms of pressure drop coefficient K by using ANSYS Fluent with three different pipes diameters and various Reynolds number Re for each mitre angle and compare the results with experimental data from decent studies.

2. SIMULATION PROCEDURE

ANSYS Fluent employed to accomplish the simulation in this work. The procedure for each examined case consisted of six main steps pre-processing steps (1-5) and post processing step (6):

1. Creating the geometry.
2. Meshing.
3. Applying the boundary conditions.
4. Setting the solver.
5. Running the solution.

6. Displaying and evaluating the results.

2.1. Geometry and Mesh Generation

The Geometry for each case study was generated by using ANSYS-15 Design Modeler ANSYS Workbench software (Guide, 2013). The geometry is three dimensional and it consists of two straight pipes (inlet and outlet sections each one has a length of 0.6m) joined together to generate the mitre bend. The length of the inlet section was selected to obtain fully developed flow upstream of the mitre bend. Three pipes' dimeters were employed in this study with pipe diameters of 1mm, 2mm and 3mm. Three different mitre angles $\alpha^* = 30^\circ$, 45°, and 60° were used for each pipe diameter. Fig. 1 depicts a schematic figure of the case geometry, where α^* is the mitre angle.

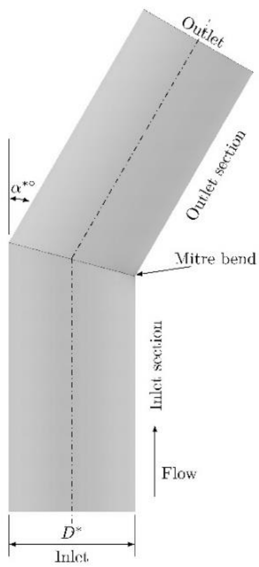

Fig. 1. Schematic Figure of the Mitre Bend Geometry.

After creating the geometry, the ANSYS Meshing software was utilised to generate the mesh. A tetrahedral with inflation mesh of 0.6mm elements size and hard behavior was employed for the inlet and the outlet sections of each case. Inflations of five layers, 1.2 rates of growth and smooth transition were utilised nearby the walls to obtain more accurate results in these areas. The size of the mesh was chosen after applying independency mesh size test. Six different mesh sizes were examined in terms of pressure drop in the inlet section. The maximum difference between the pressure values resulting from different mesh sizes was about 4.5%.

Fig. 2 clarifies the mesh specifications of the geometry nearby to the mitre-bend for the case of $\alpha^*=45^\circ$ and $D^*=3$mm.

2.2. Boundary Conditions and Solver Settings

After geometry and mesh generation, boundary conditions and solver settings were applied to the case study. The inlet surface of the bend's entrance part and outlet surface of the bends exit part were characterized as a velocity inlet and a pressure outlet respectively. Pipes walls were characterized as walls. Various flow velocities were examined in this study from 0.05 to 2.2 m/s to acquire Reynolds numbers values in a range of Re= 150-2190. After applying the boundary conditions, the appropriate solver (Fluent) should be setting. The solver settings specifications are shown in Table 1.

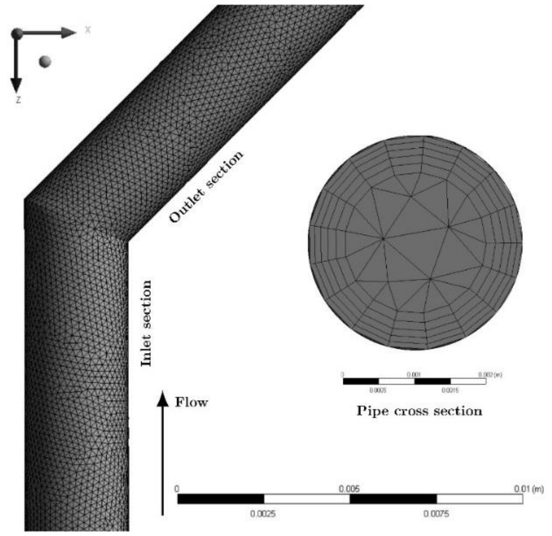

Fig. 2. Mesh Specifications Nearby the Mitre Bend and in the Cross Section for $\alpha^{*}=45^{\circ}$ and $D^{*}=3mm$.

Table1. Selected Settings of the Solver.

Solver Setting	The Selected Option
The coupling of pressure-velocity	SIMPLE
The gradient	Green-Gauss cell based
The pressure	Second order
The momentum	Second order upwind
Convergence Criteria	1×10^{-6}

Three dimensional, double precisions, steady, and pressure-based solver was applied for every case. Absolute velocity formulation was used with laminar flow model. The employed working fluid was Water liquid at atmospheric pressure and 25°C.

2.3. Running the Solution and Evaluating the Results

After finishing the solver settings, the solution for each case was accomplished by applying 600 iterations for each run to verify the convergence criteria. When the convergence obtained, the data of pressure distribution along the centerline of the inlet and outlet sections were collected. For obtaining accurate results, about 500 pressure data results were collected along each of the inlet and the outlet sections for each case. The collected results then employed to evaluate the needed data as specified in section 3.

3. PROCEDURE OF DATA CALCULATIONS

This section includes the procedures of employing the collected data from the CFD simulation to compute the required quantities in this work.

3.1. Velocity Profile

Velocity profiles evaluated at different distances from the inlet of the upstream section. At each location, velocity distribution along the radius of the pipe from r*=0 to r*=R*=D^*/2 were extracted from the simulation results. The maximum velocity of the flow U*max is computed by using:(White et al., 2011)

$$U^*_{max} = 2U^* \quad , \qquad (1)$$

where U* is the velocity of the flow.

3.2. Friction Factor and Reynolds Number

The Darcy friction factor C_f and the coefficient of pressure drop K were computed for each case by employing the pressure loss in straight pipes and across the mitre bend respectively. Friction factor was found by applying:(White et al., 2011)

$$C_f = \frac{2\,\Delta P^* D^*}{\Delta L^* \rho^* U^{*2}}, \qquad (2)$$

where C_f represents the friction factor, ΔP^* represents the pressure loss in the inlet section, D^* is the diameter of the mini pipe, ΔL^* is the length of the pipe between the two selected points, ρ^* represents the density of the fluid. The pressure drop ΔP^* was computing by subtracting the average pressure at L^*_{in} =0.4m from the average pressure at L^*_{in} =0.2m. The Reynolds number Re of the flow was computed by applying: (White et al., 2011)

$$Re = \frac{\rho^*\, U^*\, D^*}{\mu^*}, \qquad (3)$$

where μ^* is water viscosity.

3.3. Mitre Bend Pressure Loss Coefficient

The procedure of Ito (1960) was utilized to find the pressure loss throughout the mitre bend. This procedure was successfully used in various studies like Spedding and Bénard (2007), Spedding et al. (2004), Crawford et al. (2007) and Al-Tameemi and Ricco (2018) with accurate results. The procedure used the pressure distribution along the inlet section and along the outlet section to compute the pressure drop throughout the mitre bend. The difference between the pressure distribution along the inlet and outlet sections equals the drop of the pressure through the mitre bend ΔP^*_{MB}. The procedure of mitre bend pressure drop calculation is clarified in details by Al-Tameemi and Ricco (2018).

The mitre bend pressure loss ΔP^*_{MB} then utilized to calculate the coefficient of pressure drop K by using: (Munson et al., 2006)

$$K = \frac{2\,\Delta P^*_{MB}}{\rho^* U^{*2}}, \qquad (4)$$

where ΔP^*_{MB} is the pressure loss across the bend.

4. RESULTS AND DISCUSSIONS

This section includes the obtained data of pressure drop throughout mini-scale mitre bends. Various ranges of mini-tube diameters, mitre angles and Reynolds numbers were employed in this study. Pressure drop along the inlet section was utilized to compute the friction factor and verify the accuracy of the obtained data. The pressure drop along the outlet section was used with that of the inlet section to compute the pressure drop across the bends.

4.1. Inlet section pressure drop

Pressure drop in the inlet section is employed to compute the laminar flow Darcy friction factor. Before computing the friction factor C_f, it was crucial to verify the fully developed flow condition. The results of velocity profile of the flow at various locations from the entrance of the inlet section, between L^*_{in} = 0 and L^*_{in} = 0.5m, were used to prove the fully developed condition of the flow. The obtained results of velocity profiles illustrate that the condition of fully developed flow was achieved at 0.2m downstream of the entrance as depicted in Fig. 3. The velocity profiles, after that distance, are congruent at the selected distances up to L^*_{in} =0.5m.

Pressure drop along the inlet section was collected from the simulation results for every case from L^*_{in} =0.2m to L^*_{in} =0.4m and used to evaluate Darcy friction factor C_f.

A comparison between the evaluated results of Darcy friction and the empirical formula of McKeon et al. (2004) and the experimental data of Elazhary and Soliman (2012) was accomplished to verify the accuracy of the present work computed data as depicted in Fig. 4.

It can be noticed that the present work results of C_f agree with the published experimental data and well-known empirical correlation especially at Re < 1000. The computed friction factor of the present work coincides with the experimental results of Elazhary and Soliman (2012) with less than ±5 % average error. However, the present work data and the experimental data of the mini pipes follow the same trend of the empirical formula of McKeon et al. (2004), nevertheless they were higher with about ±10% average error.

The convenience agreement of the present work C_f with the experimental data more than that with the empirical correlation could be caused by the difference in the pipe scale, as both of the present work and the experimental results of Elazhary and Soliman (2012) used mini scale pipes with D^*=1.87mm, while the empirical correlation of McKeon et al. (2004) was derived according to experimental data of flow through normal size pipes with D^*=129mm. The comparison supports the present work data accuracy as they well agreed with the empirical formula and the published experimental results.

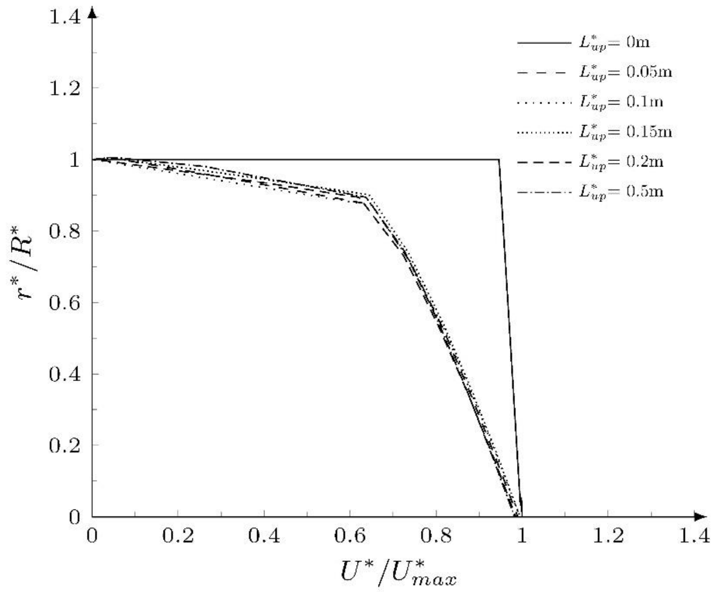

Fig. 3. Velocity Profiles at Various Distances from the Entrance Upstream of the Mitre-bend.

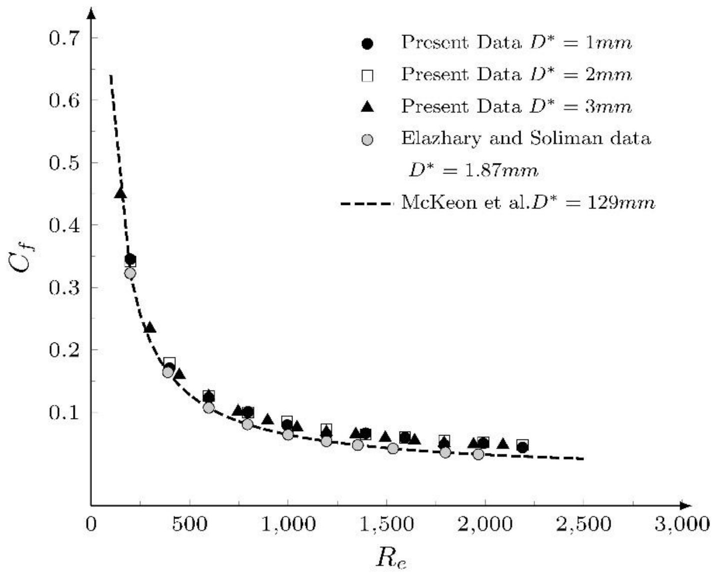

Fig. 4. Comparison Between the Present Work Darcy Friction Factor of Laminar Flow in the Straight Mini Pipes Upstream of the Bend and the Empirical Correlation of McKeon et al. (2004) and the Experimental Data of Elazhary and Soliman (2012).

4.2. Mitre bend pressure loss coefficient

Pressure drop through the bend ΔP^*_{MB} for all cases was determined by following the procedure of Ito (1960). Pressure drop coefficient K then computed by applying equation 4 for each pipe diameter and mitre angle. More than one-hundred data points of K were evaluated in this work. Figs. 5a, 6a and 7a display the pressure loss through the mitre bends of α^*=30°, 45° and 60° respectively in terms of pressure drop (ΔP^*_{MB}). It can be noticed that the pressure drop across the bend increases with the decrease of the pipe diameter and the increase of the flow velocity. Furthermore, the effect of the diameter on the pressure loss through the bend increases with the increment of the flow Reynolds number Re. This behavior of the pressure drop is expected as the pressure drop is directly proportional with the increase of the inertial forces those are increase with the increase of the flow velocity and with the decrease of the pipe diameter.

Figs 5b, 6b and 7b depict a comparison between the results of computed pressure loss coefficient K in the present work of mini mitre bends with 30°, 45° and 60° mitre angles respectively, and the experimental data of Schubart (1935) and the reported values in textbooks (Rennels, 2022, White et al., 2011).

The evaluated data show that the coefficient of the pressure drop K of mini-scale mitre bends increases with the increase of mitre angle α^* and it is approximately independent on the Reynolds number of the flow Re for the used flow velocities. The directly proportion of the coefficient K with the increase of the mitre angle α^* could be related to the flow separation and secondary flow increment with the increase of mitre angles as depicted in Fig.8.

It can be noticed that results of this work have larger values comparing with the experimental data and the reported values in text books. The difference could be related to the surface tension effect as the present work employed mini-scale pipes diameters (1-3mm) and laminar flow, while the reported values by White et al. (2011) and Rennels (2022) did not mention the flow velocity nor the pipe size, and the experimental data of Schubart (1935) used very high Reynolds numbers Re>25000 through large pipes diameter D*=43mm as the influence of surface tension is approximately negligible.

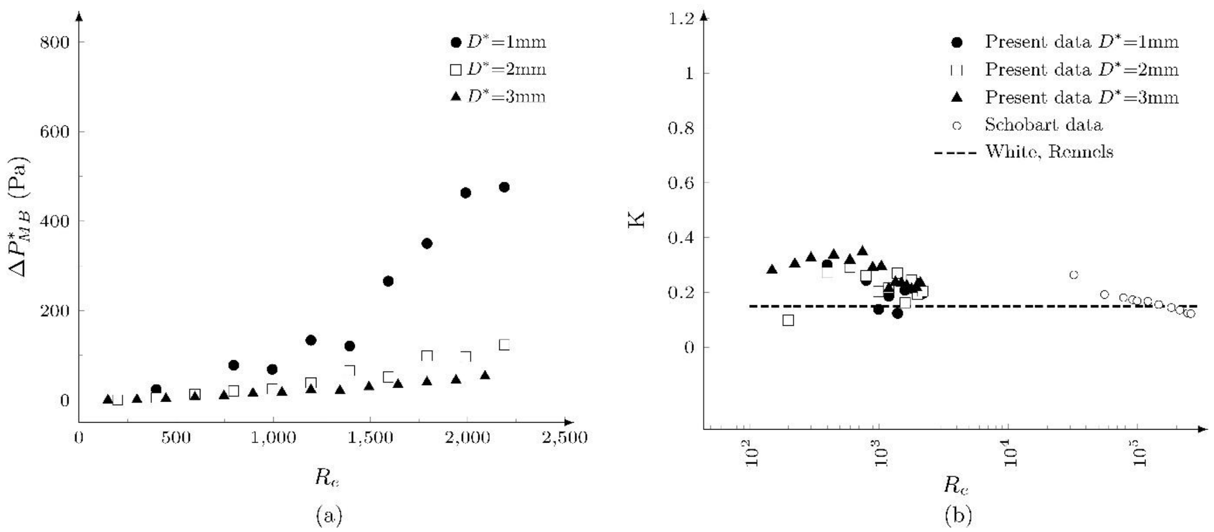

Fig. 5. (a) Pressure Drop ΔP^*_{MB} Across Mitre Bend, (b) A Comparison Between the Present Pressure Loss Coefficient K and the Experimental Data of Schubart (1935) , White et al. (2011) & Rennels (2022) for α^*=30.

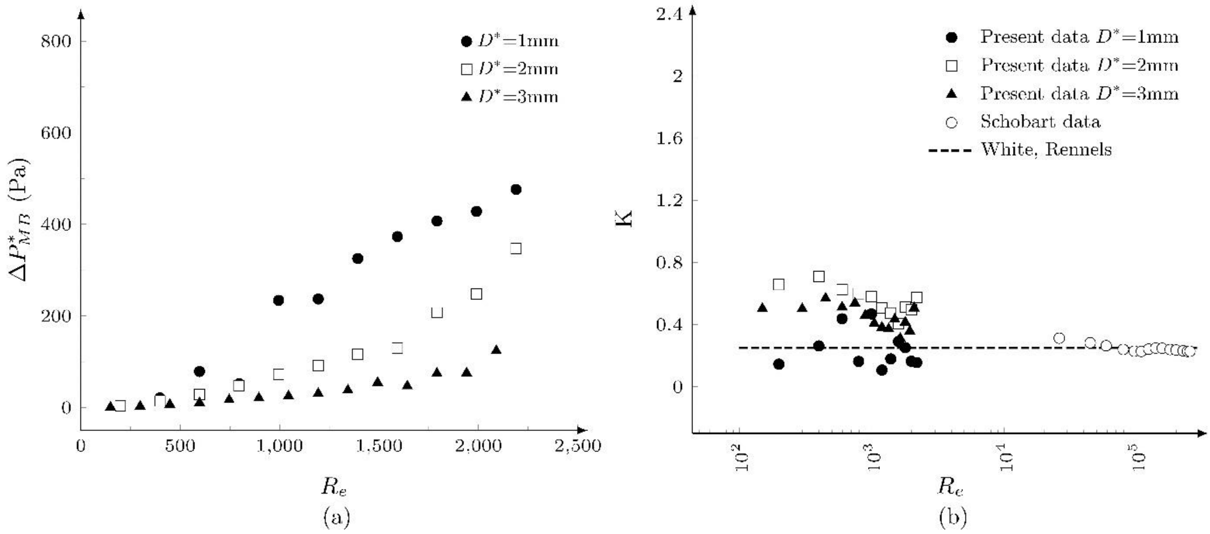

Fig. 6. (a) Pressure Drop ΔP*MB Across Mitre Bend, (b) A Comparison Between the Present Pressure Loss Coefficient K and the Experimental Data of Schubart (1935) , White et al. (2011) & Rennels (2022) for α*=45.

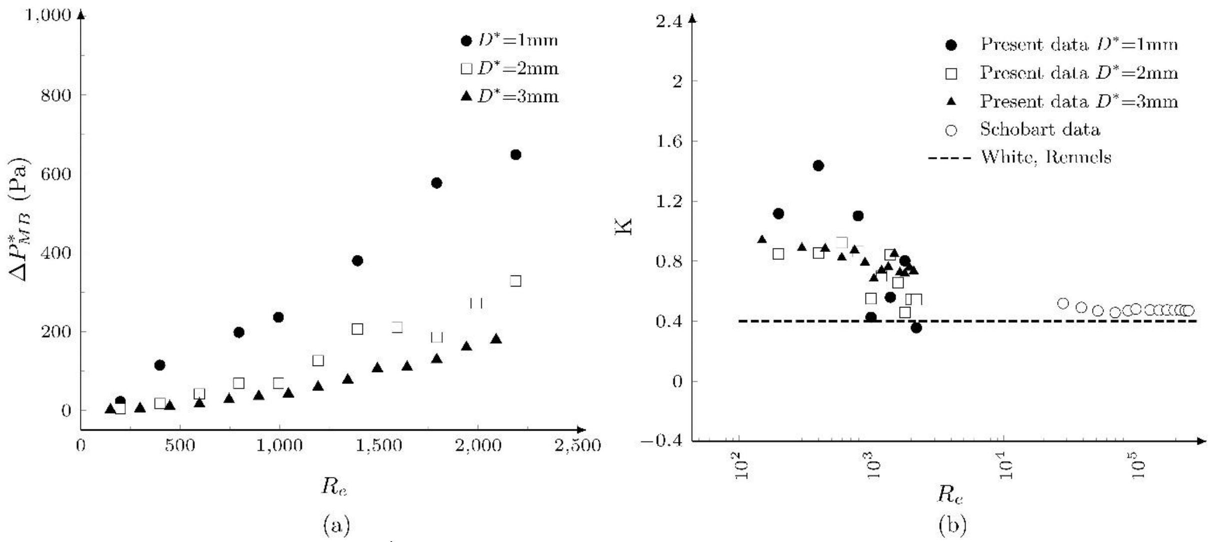

Fig. 7. (a) Pressure Drop ΔP^*_{MB} Across Mitre Bend, (b) A Comparison Between the Present Pressure Loss Coefficient K and the Experimental Data of Schubart (1935) , White et al. (2011) & Rennels (2022) for α^*=60.

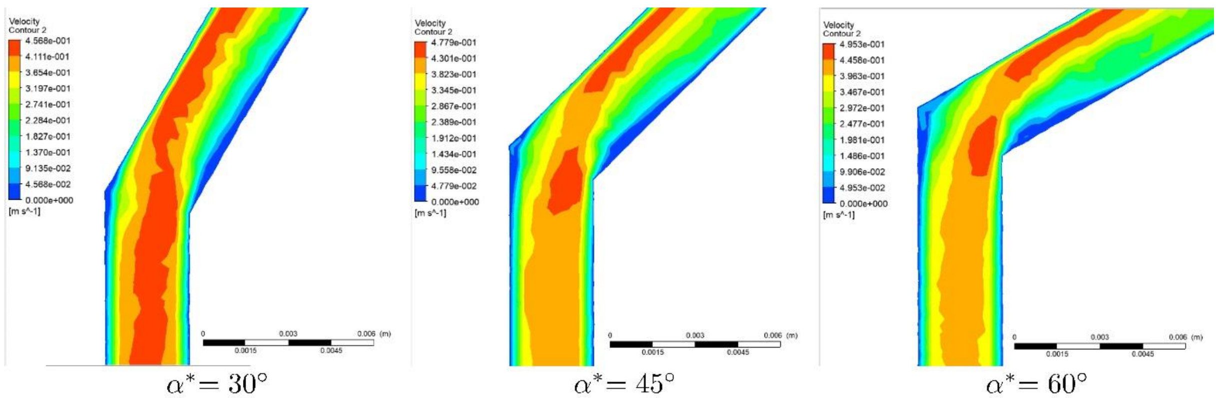

Fig. 8. Velocity contours for various mitre angles for the case of D^*=3mm and Re=1492.

New values of the coefficient K for laminar flow throughout mini-scale mitre bends were found in this study by averaged the computed values of K for each mitre angle α^*. Fig. 9 shows a comparison between the coefficient of the pressure drop values K for various mitre angles which are reported by Rennels-Hudson and White (Rennels, 2022, White et al., 2011) and the new proposed values of mini mitre bends in the present work. The comparison displays that the proposed values of the present work follow the similar trend of the reported data in the literature. However, the present results have greater values than the reported data, of large-scale pipes and high Reynolds numbers, with 39-59%. This increase could be related to the domination of surface tension over the other forces as a consequence of using mini-scale pipe sizes and laminar flow conditions in the present study.

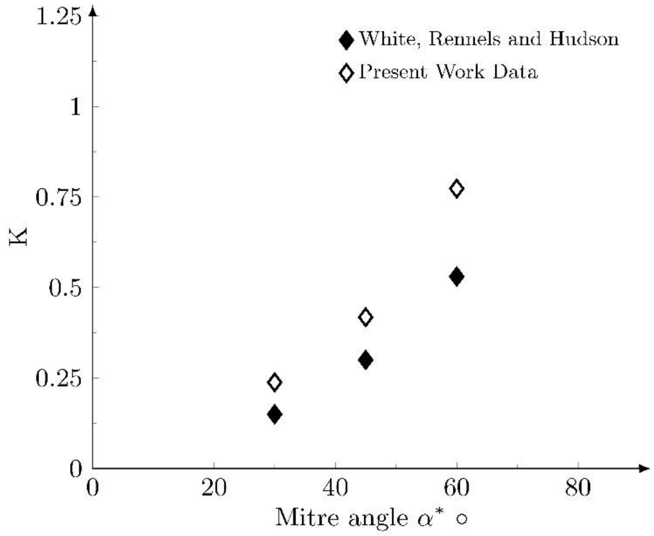

Fig. 9. Comparison Between the Reported Pressure Loss Coefficient K by Rennels-Hudson and White (Rennels, 2022, White et al., 2011) and the Average Values of the Present Work Data.

5. CONCLUSIONS

This work investigated the pressure loss coefficient of laminar flow across mini scale mitre bends by using CFD simulation. Three mini pipe diameters were used and three various mitre angles were employed for each diameter. More than 100 pressure loss data points were computed in this study in straight pipes and across the bends. The comparison between the pressure drop in straight pipes and the experimental data in the literature show an agreement within ±5% average error. It can be concluded that the pressure drop coefficient of laminar flow across mini scale mitre bends does not affect by the flow velocities and the pipes diameters for the employed boundary conditions. The obtained data show that the pressure loss through the mitre bends for the employed boundary conditions influences by the mitre angle α and this agrees with the published research in the literature. New values of laminar flow pressure loss coefficient across mini mitre bends are found and they were about 39-59% greater comparing with the reported data in the literature for normal size mitre bends. The divergence of present work data from the published data in the literature could be caused by the difference in the mitre pipes scale and the flow conditions.

6. REFERENCES

AL-SAYYAB, A. 2018. An experimental study for the effect of capillary tube diameter on refrigerator performance with new alternative refrigerant mixture to R134a. Kufa Journal of Engineering, 9, 31-44.

AL-TAMEEMI, W. T. & RICCO, P. 2018. Pressure-loss coefficient of 90 deg sharp-angled miter elbows. Journal of Fluids Engineering, 140, 061102.

CRANE 1988. Flow of fluids through valves, fittings, and pipe, Crane Company.

CRAWFORD, N., CUNNINGHAM, G. & SPENCE, S. 2007. An experimental investigation into the pressure drop for turbulent flow in 90 elbow bends. Proceedings of the Institution of Mechanical Engineers, Part E: Journal of Process Mechanical Engineering, 221, 77-88.

DEBNATH, S., BANDYOPADHYAY, T. & SAHA, A. 2017. CFD Analysis for Non-Newtonian Pseudo Plastic Liquid Flow Through Small Diameter U-BEND. Journal of Applied Fluid Mechanics, 10, 971-987.

DONALDSON, A. A., KIRPALANI, D. M. & MACCHI, A. 2011. Single and two-phase pressure drop in serpentine mini-channels. Chemical Engineering and Processing: Process Intensification, 50, 877-884.

ELAZHARY, A. & SOLIMAN, H. 2012. Experimental investigation of the two-phase flow regimes and pressure drop in horizontal mini-size rectangular test section. Archives of Thermodynamics, 33, 47-6.

GHOBADI, M. & MUZYCHKA, Y. 2014. Pressure drop in mini-scale coiled tubing. Experimental thermal and fluid science, 57, 57-64.

GUIDE, W. U. S. 2013. Software Package, Ver. 15, ANSYS. Inc., Canonsburg, Pennsylvania, USA.

HAIDAR, N. 1995. Prediction of compressible flow pressure losses in 30–150 deg sharp-cornered bends.

ITO, H. 1960. Pressure losses in smooth pipe bends.

KIM, S.-M. & MUDAWAR, I. 2013. Universal approach to predicting heat transfer coefficient for condensing mini/micro-channel flow. International Journal of Heat and Mass Transfer, 56, 238-250.

KIRCHBACH, H. 1935. Loss of energy in miter bends. Transactions of the Munich Hydraulic Institute, American Society of Mechanical Engineers, 3.

LI, X. & HIBIKI, T. 2017. Frictional pressure drop correlation for two-phase flows in mini and micro single-channels. International Journal of Multiphase Flow, 90, 29-45.

LIU, W., LONG, Z. & CHEN, Q. 2012. A procedure for predicting pressure loss coefficients of duct fittings using computational fluid dynamics (RP-1493). HVAC&R Research, 18, 1168-1181.

MCKEON, B., SWANSON, C., ZAGAROLA, M., DONNELLY, R. & SMITS, A. J. 2004. Friction factors for smooth pipe flow. Journal of Fluid Mechanics, 511, 41-44.

MILLER, D. S. 1990. Internal Flow Systems, BHRA (Information Services).

MORTAZAVI, M. & TAJIRI, K. 2015. Two-phase flow pressure drop in flow channels of proton exchange membrane fuel cells: Review of experimental approaches. Renewable and Sustainable Energy Reviews, 45, 296-317.

MUNSON, B. R., YOUNG, D. F., OKIISHI, T. H. & HUEBSCH, W. W. 2006. Fundamentals of Fluid Mechanics, John Wiley & Sons. Inc., USA.

PARMAR, S., PATEL, K. N. & JEJURKAR, A. 2017. A review of air conditioning with the use of mini-channel and micro-channel heat exchanger. Int. J. Sci. Eng. Res, 8, 86-90.

RENNELS, D. C. 2022. Pipe flow: A practical and comprehensive guide, John Wiley & Sons.

SALIH, S. M. & YASEEN, D. T. 2020. NUMERICAL MODELING OF LAMINAR FORCED CONVECTIVE ENHANCEMENT OF (AL2O3-WATER) NANOFLUIDS IN A CIRCULAR PIPE. Kufa Journal of Engineering, 11, 19-30.

SCHMANDT, B. & HERWIG, H. 2013. Loss coefficients for periodically unsteady flows in conduit components: illustrated for laminar flow in a circular duct and a 90 degree bend. Journal of fluids engineering, 135, 031204.

SCHMANDT, B. & HERWIG, H. 2016. Losses due to conduit components: An optimization strategy and its application. Journal of fluids engineering, 138, 031204.

SCHUBART, W. 1935. Energy loss in smooth-and rough-surfaced bends and curves in pipe lines. Trans. Hydraul. Inst. Munich Tech. Univ, 3, 81-99.

SPEDDING, P. & BENARD, E. 2007. Gas–liquid two phase flow through a vertical 90 elbow bend. Experimental Thermal and fluid science, 31, 761-769.

SPEDDING, P., BENARD, E. & MCNALLY, G. 2004. Fluid flow through 90 degree bends. Developments in Chemical Engineering and Mineral Processing, 12, 107-128.

SUKAMTA, S., SAPUTRA, D. A., SUDARJA, S., SUNDARI, S. & ADI, R. K. 2023. Void Fraction of Two-Phase Flow of Air–Emulsion of Water and Oil in Horizontal Mini Pipe. Journal of Advanced Research in Fluid Mechanics and Thermal Sciences, 110, 121-130.

VERSTEEG, H. & MALALASEKERA, W. 1995. Computational fluid dynamics. The finite volume method, 1-26.

WEN, J., GU, X., WANG, S., LI, Y. & TU, J. 2018. The comparison of condensation heat transfer and frictional pressure drop of R1234ze (E), propane and R134a in a horizontal mini-channel. International Journal of Refrigeration, 92, 208-224.

WHITE, F. M., NG, C. & SAIMEK, S. 2011. Fluid mechanics, McGraw-Hill, cop.

YUSOF, M., SAINAN, K. & ZAKARIA, I. 2020. Pressure Drop Analysis of Serpentine Mini Channel through Local Loss Coefficient Value. Journal of Mechanical Engineering (1823-5514), 9.

ZHANG, J., LEI, L., CHENG, C., HUANG, C., XIAO, Q., XIN, G. & WANG, M. 2023. Experimental investigations of gas–liquid two-phase flow in a horizontal mini pipe: Flow regime, void friction, and frictional pressure drops. Physics of Fluids, 35.